Computational Modelling of Motion at the Bone-Implant Interface after Total Knee Arthroplasty: The Role of Implant Design and Surgical Fit

Computational Modelling of Motion at the Bone-Implant Interface after Total Knee Arthroplasty: The Role of Implant Design and Surgical Fit

Noel Conlisk, PhD[1, 2],

Colin R. Howie, FRCS Ed (Orth)[1,3],

Pankaj Pankaj, PhD[2],

Running title: Post-TKA implant design and fit.

[1]School of Clinical Sciences,
The University of Edinburgh,
Edinburgh, UK

[2] School of Engineering,
The University of Edinburgh,
Edinburgh, UK

[3] Department of Orthopaedics,
New Royal Infirmary of Edinburgh,
Old Dalkeith Road, Little France,
Edinburgh, UK

Correspondence:

Dr. Noel Conlisk
Room E3.24,
The Queen's Medical Research Institute,
College of Medicine and Veterinary Medicine,
The University of Edinburgh,
EH16 4TJ, Edinburgh, UK
Phone: (+44) 7775 332506
Email: noel.conlisk@ed.ac.uk

ABSTRACT

Background:

Aseptic loosening, osteolysis, and infection are the most commonly reported reasons for revision total knee arthroplasty (TKA). This study examined the role of implant design features (e.g. condylar box, pegs) and stems in resisting loosening, and also explored the implants sensitivity to a loose surgical fit due to sawblade oscillation.

Methods:

Finite element models of the distal femur implanted with four different implant types; a cruciate retaining (CR), a posterior stabilising (PS), a total stabilising (TS) with short stem (12mm x 50mm), and a total stabilising (TS) with long stem (19mm x 150mm), were developed and analysed in this study. Two different fit conditions were considered; a normal fit, where the resections on the bone match the internal profile of the implant exactly, and a loose fit due to sawblade oscillation, characterised by removal of 1mm of bone from the anterior and posterior surfaces of the distal femur. Frictional interfaces were employed at the bone-implant interfaces to allow relative motions to be recorded.

Results:

Our results showed that interface motions increased with increasing flexion angle, and with loose fit. Implant design features were found to greatly influence the surface area under increased motion, while only slightly influencing the values of peak motion. Short uncemented stems behaved similar to PS implants, while long canal filling stems exhibited the least amount of motion at the interface under any fit condition.

Conclusion:

In conclusion, long stemmed prostheses appear less susceptible to surgical cut errors than short stemmed and stemless implants.

KEYWORDS: Implant design features; Surgical resections; Sawblade error; Primary knee arthroplasty; Revision knee arthroplasty; Finite element analysis.

1. INTRODUCTION

Micromotion of the tibial bearing component and failure of the tibial tray have been examined extensively using *in vitro* and *in silico* techniques [1-5]. However, currently there is a lack of corresponding studies which deal with micromotion of the femoral component, despite the fact that the difference between the number of revised tibial and femoral components as a result of aseptic loosening is less than a 3% [6]. While it is possible that a small percentage of femoral component revisions may occur in parallel to revision of a loose tibial component (to ensure conformity), it is unlikely that this factor alone would account for the majority of femoral components revised due to aseptic loosening. The reported trends with respect to loosening [6, 7] and the increasing number of revision TKAs performed each year [8] suggests that aseptic loosening of the femoral component has the potential to become a more serious clinical issue.

For ethical reasons, little information exists on the acceptable level of interfacial motion which leads to bone ingrowth vs. fibrous tissue formation and eventual loosening following TKA in humans. However, prior studies have attempted to extrapolate the upper and lower bounds of motion based on canine models [9, 10]. Pilliar et al. [9] reported that motions in excess of 150μm were disruptive to osseointegration at the prosthesis bone interface and led to the formation of fibrous tissue. A subsequent more comprehensive *in vivo* study, again using a canine model, placed the lower bound of motion for this fibrous tissue phase at 40μm [10]. On the other hand low levels of motion at the bone implant interface (< 40μm) may be beneficial in promoting bone ingrowth into the prosthesis and increase stability through a strong bond between prosthesis and bone [11, 12].

Early indications of loosening and implant failure in humans are observed clinically by tracking changes in the position and orientation of the implant over time through examination of

X-rays or through more specialised techniques such as radio stereo photogrammetric analysis (RSA) [13-16]. However, such techniques are typically limited to tracking values of inducible motion or permanent migration which exceed 100μm [16-19], and are unable to resolve the relatively small interfacial motions (40 – 100μm) which play a key role in particle induced osteolysis [14] and aseptic loosening of the implant.

It is recognised that fixation method (cemented or uncemented) and implant configuration (e.g. stemmed or stemless) can exert a large influence on the global motions between bone and implant [20-23]. Recent studies have suggested that implant design features such as size and placement of distal femoral pegs [24], anterioposterior slope of the femoral component [25], and angle of fit of the implant [26], may also play a role in the long term survival of the prosthesis.

Another factor which may influence clinical outcomes is sawblade oscillation. Undesirable motion of the saw blade during operation can lead to errors in femoral cuts [27-29], where displacement of the free end of the saw blade is a function of blade thickness, e.g. increasing blade thickness reduces displacement [29]. Out of plane motion of the saw blade in combination with displacement of pinned cutting blocks during surgery has been found to result in surgical cut errors of the range of 0.8 – 1.2mm [27, 28, 30], leading to a less than optimal positioning of the prosthesis and potentially compromising the long term survival of the implant.

As a result the aims of the current study were:

- To determine the influence of implant features such as; pegs, condylar box sections, and stems, on motion at the bone-implant surface for an uncemented femoral component.
- To examine which of these implant configurations were more resistant to a loose fit scenario.

We hypothesised that implant design features play a key role in determining the magnitude and distribution of motion at the bone-implant interface and that motions for all implants would increase in the presence of a loose fit.

2. MATERIALS AND METHODS

2.1 Geometry:

This study used a virtual representation [31] of the large left fourth generation composite femur (Sawbones; Pacific Research Laboratories, Vashon, Washington) implanted with four different implant types as shown in Fig. 1: (a) a cruciate retaining implant (CR), (b) a posterior stabilising implant (PS), (c) a total stabilising implant with short stem (TSSS) (12mm x 50mm), and (d) a total stabilising implant with long stem (TSLS) (19mm x 150mm) from the Triathlon® series product line (Stryker®, Newbury, United Kingdom). Computer aided design software (Autodesk Inventor™ 2010, Autodesk Inc., San Rafael, CA), in conjunction with surgical template measurements were used to develop 3D models of each femoral implant investigated, and to carry out surgical resections on the femur for virtual implantation.

2.2 Implant fit conditions:

Two different fit conditions were developed, as shown in Fig. 2: (a) a perfect fit between the internal geometry of the implant and the femoral bone cuts and (b) a simulated loose fit between bone and implant, where the loose fit was characterised by excessive removal of material to a depth of 1mm from both the anterior and posterior surfaces of the femur due to saw blade oscillation. These two conditions of fit were then applied to all stemless and stemmed implant scenarios investigated in this study.

2.3 Interface properties:

In this study, all FE analyses were conducted in Abaqus (Abaqus 6.10-1, Dassault Systemes, Simulia, Providence, RI, USA). Frictional interfaces were required to fully characterise the non-bonded femoral component interactions typically encountered following aseptic loosening. Coulomb friction was implemented at all bone-implant interfaces, with a frictional coefficient of $\mu = 0.3$ representing an average of the reported values in literature [32-35]. In Abaqus, an allowable elastic slip of $y_i = 0.005$ (or $5\mu m$) was specified directly thus ensuring numerically predicted motions were independent of mesh density, and that numerical errors due to elastic slip would be of a relatively small magnitude compared to the motions being measured. In addition to these settings, several other software specific parameters were required for contact analyses conducted in Abaqus, details of these parameters, and their respective values as applied in the current analyses, can be found in the supplementary text (Supplement A).

2.4 Material properties, loading and boundary conditions:

All materials were assumed to be linear elastic and isotropic, as has been done in many previous studies [21, 36, 37]. Elastic constants used for each structure are presented in Table 1. In this study, three functional flexion angles (0°, 22°, 48°) during the stance phase of gait for ascending stairs were investigated. Each flexion angle was modelled as a static load step. The loads acting on the femur in each instance were comprised of six separate components: the patella-femoral force (PF); the medial and lateral components of the joint normal force (Fm and Fl); the medial and lateral components of the joint shear force (APm and APl); and the internal/external moment (IE). The exact magnitudes applied for each component of force are indicated in Table 2. All forces were applied as distributed pressure loads over realistic contact

areas [37], with a 60-40% (medial/lateral) load distribution acting across the condyles assumed for the axial components of force [24, 38].

To ease the computational cost associated with frictional interfaces, each femur model was truncated at the mid-diaphysis and all its translations/rotations fixed. Based on initial investigations, an optimum distance of 242mm from the distal most point on the condyles was selected. This manner of fixation is consistent with numerous previous FE [21, 23, 37, 39-42] and experimental investigations [20, 36, 40, 43]. In addition by reducing the overall geometrical size of the model by half, a higher resolution mesh could then be applied without significant increase in computational run time. Final FE meshes typically comprised of approximately 290,000 to 390,000 linear tetrahedral elements (C3D4) depending on implant type, with a maximum allowable edge length of 2mm for all models (note: element edge lengths were further refined around key regions of interest, e.g. the femoral pegs of the CR implant). All simulations were performed on a dual core Intel i5 laptop with 8GB of RAM. Simulation runtime varied from 2hrs to 2.5hrs depending on model complexity (i.e. stemless vs. stemmed models).

2.5 Characterisation of motion at the interface:

The relative motion of each implant to the bone was described using three built in parameters in Abaqus. The first (Copen) describes the relative separation of two surfaces in the normal direction (i.e. normal to the femoral cuts), the second (Cslip 1) and third (Cslip 2) represent micromotions tangential to the contact surfaces in two orthogonal directions.

3. RESULTS

3.1 Stemless and stemmed prostheses under normal fit conditions:

At 48° flexion (Fig. 3) the CR implanted femur experienced the majority of motion on the anterior chamfer, whereas for the PS implanted femur the largest area of motion was located on the distal aspect of the medial femoral condyle. Separation of the bone and implant surfaces as defined by Copen was found to be largest on the anterior surface in the CR implanted femur and on the medial aspect of the intercondylar box in the PS implanted femur. The variation of these parameters with increasing flexion angle can be seen in the supplementary text (Supplement B, Fig. B.1 – B.2). At lower flexion angles, all components of motion for both CR and PS implanted femurs were found to be well below $40\mu m$, and in some cases below $25\mu m$. At higher flexion angles, however, the differences due to implant design features became more noticeable. In general, the majority of motions for both implant types were found to be well below the limit for osseointegration. However, small portions of the anterior chamfer in the CR implanted femur and the distal surface in the PS implanted femur were found to experience levels of motion within the fibrous tissue formation region, e.g. motions in the range of $40 – 80\mu m$, at 48° flexion. Though peak values were of a similar magnitude for both implant types (Fig. 4), the implant design features are found to result in distinct differences in the surface areas that experienced relative motions (Table 3 – Table 5). In particular, at 48° flexion the PS implanted femur was subjected to increased motion ($40 – 80\mu m$) over a surface area almost 50% larger than that experienced by the CR implanted femur (Table 5). However, it must be noted that in the Cslip 2 direction, the surface area associated with motion for the CR implant was greater than that associated with the PS implant (though much lower levels of motion were observed in this direction).

Contour plots for the different components of interface motion (Copen, Cslip 1 and Cslip 2) at 48° flexion were also generated (Fig. 5) for the stemmed implants. The figure compares

motion at the interface for both the TSSS (12mm x 50mm) and the TSLS (19mm x150mm) implanted femurs. By comparing Fig. 5 and Fig. 3, it can be seen that the TSSS implanted femur exhibited a similar distribution of motion to the PS implanted femur, though it should be noted that the addition of a fully frictional short stem led to a slight reduction of motion on both the distal surface of the femur and the distal aspect of the intercondylar box when compared with a stemless PS implanted femur. The addition of a long stemmed femoral component (TSLS), on the other hand, was found to result in peak motions below all other implants, typically less than $38\mu m$ in peak areas and less than $20\mu m$ over the majority of the distal surface. The long stemmed femoral component also consistently exhibited the lowest surface area associated with increased motion for each of the flexion angles tested (Table 4 and Table 5). Additional contour plots at 0° and 22° flexion can be seen in the supplementary text (Supplement B, Fig. B.5 – B.6).

3.2 Stemless and stemmed prostheses under loose fit conditions:

From the graphs of peak motion (Fig.4) and the 3D contour plots of interface relative motion (Fig. 6), it can be seen that in general poor implant fit caused an increase in motion. From Fig. 3 and Fig.6, it can also be seen that the loose fit condition had a more significant impact on the PS implanted femur than the CR implanted femur. In the CR implanted femur, there was a slight increase in the surface area associated with peak motions on the anterior chamfer (Cslip 1). In comparison, the PS implanted femur showed an increase in all three components of interfacial motion (Copen, Cslip 1 and Cslip 2), a large proportion of which was in the band for fibrous tissue formation ($40 - 80\mu m$) (Table 5). Furthermore, a portion of the medial aspect of the intercondylar box and the anterior chamfer experienced motions in excess of $80\mu m$ under loose fit conditions. Additional contour plots at 0° and 22° flexion can be seen in the supplementary

text (Supplement B, Fig. B.3 – B.4).

Interestingly, the femur implanted with a short stemmed femoral component (TSSS) was found to exhibit increased motion in the upper limit of the fibrous tissue formation range, e.g. >80μm. However, it can be observed by comparing Fig.7 and Fig.6 that the stem, much like the femoral pegs in the CR implanted femur, served to resist translational motion thereby reducing the level of relative motion in the direction of Cslip 2, this was particularly noticeable on the distal surface of the intercondylar box. The TSLS implanted femur, on the other hand, showed the greatest reduction in motion under both normal and loose fit conditions. Under loose fit conditions, it was observed that the addition of a long stem lead to motions comparable to that of a PS implant under normal fit conditions (with minor regional variations). Peak motions for the TSLS implanted femur under loose fit conditions were approximately 70μm at 48° flexion (Fig. 4), however, the majority of motions on the anterior chamfer and distal femoral surface remained below 55μm. Additional contour plots at 0° and 22° flexion can be seen in the supplementary text (Supplement B, Fig. B.7 – B.8).

4. DISCUSSION

In this study, computational models of the distal femur following stemless (CR and PS) and stemmed (TS with short and long stems) TKA were developed. The influence of their different implant design features on micromotion at the bone-implant interface was then tested. Subsequently, the impact on motion at the interface due to a loose fit scenario (due to sawblade oscillation during surgery) was also considered.

The stemless implants investigated in this study represent two common industry standards in terms of implant design features (i.e. pegs or box). As in many previous studies,

micromotions at the interfaces of both implants were found to increase with increasing flexion angle [20, 44, 45]. The average interface motions for each implant remained well below the recommended limits for osseointegration at 0° and 22°. However, at 48° flexion small regions of motion at the interface were observed to enter the range for fibrous tissue formation (40 – 150μm). Interestingly, while peak motions were of a similar magnitude for both the CR and PS implants (78μm vs. 79μm) the locations of peak motions were found to vary considerably between implants; on the anterior chamfer for the CR implanted femur and the distal surface for the PS implanted femur. These regional differences between implants may have important implications for optimising implant designs to improve fixation. However, it is important to note that the similarity in peak motions between implant types suggests that implant design features may not be a dominant factor in determining the overall magnitude of motion an implant experiences. On the other hand, implant design features are found to play an important role in how interfacial motions are distributed across the interface, as evidenced by the increased surface area of motion associated with the PS implant which may indicate a higher risk of loosening in comparison to the CR implanted femur. Loosening over a greater surface area may expose the underlying bone to wear debris from the joint, thereby reducing the likelihood of bone ingrowth. Moreover, due to the presence of the femoral box section in the PS implant, the effects of loosening may not be readily apparent from standard two-plane radiographs [46], particularly when largely confined to a single condyle as reported in the present study. This may lead to an increased risk of osteolysis induced bone loss and eventual failure of the component if untreated.

The influence of stemmed femoral components was also investigated in this study. It was observed that slight differences occur in the location of peak motions when comparing the PS implanted femur with the short stemmed TS implanted femur, however, in general the short stem

was found to reduce the levels of motion at the interface by approximately 9.78% (Cslip 1 max). An *in vitro* study by Conlisk et al. [20] reported a similar reduction (9.77%) in relative motion when comparing a PS implanted femur and a TSSS implanted femur under uncemented conditions. In the present study, the addition of a long stem was found to significantly reduce distal motions, by approximately 40% (Cslip 1 max), in comparison to the other two implant types (PS and TSSS). An FE study by Completo et al. [21] reported similar trend in reduction of motions (up to 41%) when comparing contact separation at the interface for a prosthesis with press-fit stem, and no stem.

This study also investigated variations in fit through introduction of a loose fit at the bone-implant interface characterised by excessive removal of material due to saw blade motion. By comparing interface motions at 48° flexion for both normal and loose fit conditions it was observed that the PS implant was more sensitive to changes in fit conditions than the CR implant. It is expected that this difference would again become more dramatic as flexion angle increases in more strenuous activities such as deep knee bend, squatting and sitting down into a chair, e.g. activities where the defect gap would become compressed. By comparing the relatively small change in interfacial motion for a TS implant with long stem under normal (Fig.5) and loose fit conditions (Fig.7), the present study lends qualitative support to the argument that adding a stem helps to reduce interfacial motion [47], particularly in the presence of imperfect surgical cuts. In the present study for example it was observed that the short fully frictional stem led to motions comparable to that of the PS implanted femur, whereas, the long stemmed implant, on the other hand, resulted in the smallest interfacial motions which only marginally increased with imperfect surgical cuts (overall motions remained well below the normal fit PS implanted femur). It is important to note that alterations to stem length and fixation

method could impact upon this conclusion. Had the short or long stem models been cemented (e.g. fixed along the stem) it is expected that much lower interfacial motions would have been observed [20].

Only interfacial motions were examined in this study. However, the stress distribution in the femur following stemless and stemmed implantation also plays a role in the long term stability of the implant. Prosthesis induced stress-shielding is commonly observed following implantation [23, 42, 48-51], with the pattern and severity of bone loss differing with different implant types and fixation [23, 24, 39, 42]. While the long stemmed implant investigated here exhibited the lowest levels of motion and was found to be least sensitive to surgical cut errors, the presence of a long diaphyseal engaging stem may lead to greater bone loss over time in comparison to a stemless implant [21, 23]. Should sufficient loosening of the implant occur distally due to prosthesis induced bone loss at the interface, then the majority of the joint reaction force would be transmitted solely through the prosthesis [37]. In stemmed implants this can lead to a particularly devastating fatigue failure of the prosthesis at modular junctions and fracturing of the distal femur [52-54]. This reinforces the importance of achieving optimal fixation distally so as to avoid undesirable levels of motion and potentially long term fatigue failure of the prosthesis.

This study has some limitations. One limitation of the current models was with respect to the low flexion angles tested. In short, these flexion angles were not extreme enough to fully compress the defect. Had higher flexion angles been considered, it is likely that a more dramatic difference would have been observed between implants, such as where defects to the surgical cuts on the posterior condyles have been reported clinically to shift the femoral component into flexion during high flexion activities [47]. For simplicity only two stem configurations were

considered in the present study. These two stems were selected on the basis of representing opposite ends of the available product range in terms of both stem diameter and length. It is therefore expected that all other stems in the range would lie somewhere between the performance of these two, though future studies should be conducted to verify the performance of other configurations. Another consideration is that synthetic bone properties were used, while these are within the range of normal bone properties, they tend toward the lower end of the scale. To assess the significance of their impact on the conclusions drawn here, a sensitivity analysis was conducted where the cancellous bone properties were varied in 50MPa increments from 55MPa to 505MPa (in an attempt to cover the range of physiological values commonly reported). The outcomes of these analyses are presented in supplement C. These findings highlight that while the overall magnitude and distribution of motions is sensitive to large changes in cancellous material properties, the observed trends with respect to implant type and fit condition remain valid due to the comparative nature of this study. The time-independent linear elastic results presented here can be considered to represent the immediate post-operative period following implantation. For a more realistic evaluation of long-term outcomes (e.g. loosening to failure), it would be necessary to include more complex factors such as; an envelope of loading to account for all the activities of daily life over an extended period [55], an advanced remodelling framework to capture bone adaptation and ingrowth [56], and the viscoelastic/viscoplastic properties of bone [57] to adequately capture its time-dependent behaviour in response to implantation. One final consideration is that the majority of current TKA cases in both the US and UK currently employ cemented stems [7, 8]. As mentioned previously, only the effect of uncemented (frictional) stems were investigated in this study, as such it must be considered that the stemmed models presented here represent a scenario where

fixation of the prosthesis is not fully achieved, and are therefore a somewhat extreme case.

Despite these limitations, the findings of this study may aid surgeons in achieve better post-implantation outcomes, through an enhanced understanding of what role geometric features of the implants play in preventing loosening, combined with the knowledge of which implant types are more susceptible to sawblade induced errors in fit. For example, if a good metaphyseal fit is not achieved then the use of a long stem is recommended to promote implant stability and reduce the risk of loosening. Similarly the finding that pegs may be a more desirable design feature than an intercondylar box, in terms of resisting interfacial motions, holds relevance for implant designers and might inform future femoral component designs.

5. CONCLUSION

In conclusion, while this study has shown that implant design features only marginally influence peak motions in stemless implants, it has also shown that they exert a large influence on the surface area under increased motion. This finding may have serious implications for osseointegration and long term implant stability following stemless TKA. Additionally, stemmed prostheses have been found to be less sensitive to surgical cut errors than stemless implants, with the long stem providing the most resistance to cut errors, as evidenced by the greatest reduction in motion (under both fit conditions). This significant reduction in motions compared to other implant types is likely due to the large diameter canal filling stem aiding in alignment of the prosthesis and component stability in instances of loose fit. However, it is worth noting that if the prosthesis becomes reliant on the stem to maintain position in the absence of adequate bone support distally, this may increase the likelihood of prosthesis failure.

ACKNOWLEDGEMENTS:

Competing interests: None declared

Funding: Financial support from the Lothian University Hospitals NHS Trust Brown and Ireland Estates Fund and The University of Edinburgh is gratefully acknowledged. These sources had no direct involvement in study design; in the collection, analysis and interpretation of data; in the writing of the report; or in the decision to submit the article for publication.

Ethical approval: Not required

REFERENCES:

[1] Chong DYR, Hansen UN, van der Venne R, Verdonschot N, Amis AA. The influence of tibial component fixation techniques on resorption of supporting bone stock after total knee replacement. Journal of Biomechanics. 2011;44:948-54.

[2] Completo A, Fonseca F, Simoes JA. Strain shielding in proximal tibia of stemmed knee prosthesis: Experimental study. Journal of Biomechanics. 2008;41:560-6.

[3] Completo A, Simões JA, Fonseca F, Oliveira M. The influence of different tibial stem designs in load sharing and stability at the cement–bone interface in revision TKA. The Knee. 2008;15:227-32.

[4] Hashemi A, Shirazi-Adl A. Finite Element Analysis of Tibial Implants — Effect of Fixation Design and Friction Model. Computer Methods in Biomechanics and Biomedical Engineering. 2000;3:183-201.

[5] McLean AJ. The Effect of Modular Stems and Cement Fixation Techniques on the Initial Stability of the Tibial Prosthesis and the Strain Distribution within the Proximal Tibia in Primary and Revision Total Knee Arthroplasty: The University of Edinburgh; 2007.

[6] AOA. Annual Report. Adelaide: Australian Orthopaedic Association National Joint Registry; 2011.

[7] NJR. 12th Annual Report. National Joint Registry for England and Whales, Northern Ireland and the Isle of Man. 2015.

[8] Nguyen LC, Lehil MS, Bozic KJ. Trends in total knee arthroplasty implant utilization. J Arthroplasty. 2015;30:739-42.

[9] Pilliar RM, Lee JM, Maniatopoulos CD. Observations on the Effect of Movement on Bone Ingrowth into Porous-Surfaced Implants. Clinical Orthopaedics & Related Research July. 1986;208:108-13.

[10] Bragdon CR, Burke D, Lowenstein JD, O'Connor DO, Ramamurti B, Jasty M, et al. Differences in stiffness of the interface between a cementless porous implant and cancellous bone in vivo in dogs due to varying amounts of implant motion. The Journal of Arthroplasty. 1996;11:945-51.

[11] Suárez DR, Nerkens W, Valstar ER, Rozing PM, van Keulen F. Interface micromotions increase with less-conforming cementless glenoid components. Journal of Shoulder and Elbow Surgery. 2012;21:474-82.

[12] Vandamme K, Naert I, Geris L, Sloten JV, Puers R, Duyck J. The effect of micro-motion on the tissue response around immediately loaded roughened titanium implants in the rabbit. European Journal of Oral Sciences. 2007;115:21-9.

[13] Kärrholm J. Roentgen stereophotogrammetry: Review of orthopedic applications. Acta Orthopaedica. 1989;60:491-503.

[14] Nilsson KG, Kärrholm J. RSA in the assessment of aseptic loosening. Journal of Bone & Joint Surgery, British Volume. 1996;78-B:1-3.

[15] Nilsson KG, Karrholm J, Ekelund L, Magnusson P. Evaluation of micromotion in cemented vs uncemented knee arthroplasty in osteoarthrosis and rheumatoid arthritis. Randomized study

using roentgen stereophotogrammetric analysis. The Journal of Arthroplasty. 1991;6:265-78.

[16] Selvik G. Roentgen stereophotogrammetry. Acta Orthopaedica. 1989;60:1-51.

[17] Allen MJ. Functional micromechanics: moving beyond migration in evaluation of implant fixation. J Am Acad Orthop Surg. 2011;19:242-4.

[18] Nilsson KG, Kärrholm J, Linder L. Femoral component migration in total knee arthroplasty: Randomized study comparing cemented and uncemented fixation of the Miller-Galante I design. Journal of Orthopaedic Research. 1995;13:347-56.

[19] Ryd L. Micromotion in knee arthroplasty. Acta Orthopaedica. 1986;57:3-80.

[20] Conlisk N, Gray H, Pankaj P, Howie CR. The influence of stem length and fixation on initial femoral component stability in revision total knee replacement. Bone and Joint Research. 2012;1:281-8.

[21] Completo A, Simões JA, Fonseca F. Revision total knee arthroplasty: The influence of femoral stems in load sharing and stability. The Knee. 2009;16:275-9.

[22] van Loon CJM, Kyriazopoulos A, Verdonschot N, de Waal Malefijt MC, Huiskes R, Buma P. The role of femoral stem extension in total knee arthroplasty. Clin Orthop Rel Res. 2000:282-9.

[23] van Lenthe GH, Willems MMM, Verdonschot N, de Waal Malefijt MC, Huiskes R. Stemmed femoral knee prostheses: effects of prosthetic design and fixation on bone loss. Acta Orthopaedica Scandinavica. 2002;73:630.

[24] Shi J. Finite element analysis of total knee replacement considering gait cycle load and malalignment: University of Wolverhamption; 2007.

[25] Bollars P, Luyckx JP, Innocenti B, Labey L, Victor J, Bellemans J. Femoral component loosening in high-flexion total knee replacement. Journal of Bone & Joint Surgery, British

Volume. 2011;93-B:1355-61.

[26] Kluess D, Bergschmidt P, Mueller I, Mittelmeier W, Bader R. Influence of the distal femoral resection angle on the principal stresses in ceramic total knee components. The Knee. 2012;19:846-50.

[27] Bäthis H, Perlick L, Tingart M, Perlick C, Lüring C, Grifka J. Intraoperative cutting errors in total knee arthroplasty. Arch Orthop Trauma Surg. 2005;125:16-20.

[28] Plaskos C, Hodgson AJ, Inkpen K, McGraw RW. Bone cutting errors in total knee arthroplasty. The Journal of Arthroplasty. 2002;17:698-705.

[29] Yau WP, Chiu KY. Cutting errors in total knee replacement: assessment by computer assisted surgery. Knee Surg Sports Traumatol Arthr. 2008;16:670-3.

[30] Otani T, Whiteside LA, White SE. Cutting errors in preparation of femoral components in total knee arthroplasty. The Journal of Arthroplasty. 1993;8:503-10.

[31] Fourth generation femur model, BEL Repository. (2008). Available from: http://www.biomedtown.org/biomed_town/LHDL/Reception/datarepository/repositories/BEL/repository/wh_view.

[32] Abdul-Kadir MR, Hansen U, Klabunde R, Lucas D, Amis A. Finite element modelling of primary hip stem stability: The effect of interference fit. Journal of Biomechanics. 2008;41:587-94.

[33] Kuiper JH, Huiskes R. Friction and stem stiffness affect dynamic interface motion in total hip replacement. Journal of Orthopaedic Research. 1996;14:36-43.

[34] Rancourt D, Shirazi-Adl A, Drouin G, Paiement G. Friction properties of the interface between porous-surfaced metals and tibial cancellous bone. Journal of Biomedical Materials Research. 1990;24:1503-19.

[35] Viceconti M, Muccini R, Bernakiewicz M, Baleani M, Cristofolini L. Large-sliding contact elements accurately predict levels of bone–implant micromotion relevant to osseointegration. Journal of Biomechanics. 2000;33:1611-8.

[36] Completo A, Fonseca F, Simões JA. Experimental validation of intact and implanted distal femur finite element models. Journal of Biomechanics. 2007;40:2467-76.

[37] Conlisk N, Howie CR, Pankaj P. The role of complex clinical scenarios in the failure of modular components following revision total knee arthroplasty: A finite element study. Journal of Orthopaedic Research. 2015;33:1134 - 41.

[38] Burstein AH. Fundamentals of Orthopaedic biomechanics. Baltimore: Williams & Wilkins; 1994.

[39] Barink M, Verdonschot N, de Waal Malefijt M. A different fixation of the femoral component in total knee arthroplasty may lead to preservation of femoral bone stock. Proceedings of the Institution of Mechanical Engineers, Part H: Journal of Engineering in Medicine. 2003;217:325-32.

[40] Bougherara H, Zdero R, Mahboob Z, Dubov A, Shah S, Schemitsch EH. The biomechanics of a validated finite element model of stress shielding in a novel hybrid total knee replacement. Proceedings of the Institution of Mechanical Engineers Part H-Journal of Engineering in Medicine. 2010;224:1209-19.

[41] Tissakht M, Ahmed AM, Chan KC. Calculated stress-shielding in the distal femur after total knee replacement corresponds to the reported location of bone loss. Journal of Orthopaedic Research. 1996;14:778-85.

[42] van Lenthe GH, de Waal Malefijt MC, Huiskes R. Stress shielding after total knee replacement may cause bone resorption in the distal femur. Journal of Bone & Joint Surgery,

British Volume. 1997;79-B:117-22.

[43] Moran MF. Computational and experimental assessment of total knee motion: The Pennsylvania State University; 2005.

[44] Wackerhagen A, Bodem F, Hopf C. The effect of cement fixation on initial micromotion of the femoral component in condylar knee replacement. International Orthopaedics. 1992;16:25-8.

[45] Berahmani S, Janssen D, Wolfson D, de Waal Malefijt M, Fitzpatrick CK, Rullkoetter PJ, et al. FE analysis of the effects of simplifications in experimental testing on micromotions of uncemented femoral knee implants. Journal of Orthopaedic Research. 2015:n/a-n/a.

[46] Nadaud MC, Fehring TK, Fehring K. Underestimation of osteolysis in posterior stabilized total knee arthroplasty. The Journal of Arthroplasty. 2004;19:110-5.

[47] King TV, Scott RD. Femoral component loosening in total knee arthroplasty. Clin Orthop Relat Res. 1985:285-90.

[48] Conlisk N, Howie CR, Pankaj P. An efficient method to capture the impact of total knee replacement on a variety of simulated patient types: A finite element study. Medical Engineering & Physics. 2016;38:959-68.

[49] Saari T, Uvehammer J, Carlsson LV, Regnér L, Kärrholm J. Posterior stabilized component increased femoral bone loss after total knee replacement. 5-year follow-up of 47 knees using dual energy X-ray absorptiometry. The Knee. 2006;13:435-9.

[50] Soininvaara TA, Miettinen HJA, Jurvelin JS, Suomalainen OT, Alhava EM, Kröger HPJ. Periprosthetic femoral bone loss after total knee arthroplasty: 1-year follow-up study of 69 patients. The Knee. 2004;11:297-302.

[51] Spittlehouse AJ, Getty CJ, Eastell R. Measurement of bone mineral density by dual-energy x-ray absorptiometry around an uncemented knee prosthesis. The Journal of Arthroplasty.

1999;14:957-63.

[52] Issack PS, Cottrell JM, Delgado S, Wright TM, Sculco TP, Su EP. Failure at the Taper Lock of a Modular Stemmed Femoral Implant in Revision Knee Arthroplasty. The Journal of Bone & Joint Surgery. 2007;89:2271.

[53] Lim L-A, Trousdale RT, Berry DJ, Hanssen AD. Failure of the stem–condyle junction of a modular femoral stem in revision total knee arthroplasty: A report of five cases. The Journal of Arthroplasty. 2001;16:128-32.

[54] Nikolopoulos DD, Polyzois IG, Magnissalis EA, Bernard PF, Michos IV. Fracture at the stem–condylar junction of a modular femoral prosthesis in a varus–valgus constrained total knee arthroplasty. Knee Surg Sports Traumatol Arthr. 2012;20:1071-4.

[55] Geraldes DM, Modenese L, Phillips ATM. Consideration of multiple load cases is critical in modelling orthotropic bone adaptation in the femur. Biomechanics and Modeling in Mechanobiology. 2016;15:1029-42.

[56] Ruimerman R, Hilbers P, van Rietbergen B, Huiskes R. A theoretical framework for strain-related trabecular bone maintenance and adaptation. Journal of Biomechanics. 2005;38:931-41.

[57] Xie S, Manda K, Wallace RJ, Levrero-Florencio F, Simpson AHRW, Pankaj P. Time Dependent Behaviour of Trabecular Bone at Multiple Load Levels. Annals of Biomedical Engineering. 2017:1-8.

[58] Bergmann G (2008) Orthoload. Charite – Universitaetsmedizin Berlin. Available from: http://www.OrthoLoad.com

[59] Taylor SJG, Walker PS, Perry JS, Cannon SR, Woledge R. The forces in the distal femur and the knee during walking and other activities measured by telemetry. The Journal of Arthroplasty. 1998;13:428-37.

LEGEND TO FIGURES:

Fig. 1: Computer aided design model of a) a CR implant, b) a PS implant, c) a TS implant with 12mm x 50mm stem and d) a TS implant with 19mm x 150mm stem.

Fig. 2: Two-dimensional illustration of the two interface conditions considered, where a) represents a normal or "perfect" fit and b) a loose fit due to excessive removal of bone from the anterior and posterior surfaces.

Fig. 3: Femoral component relative motion expressed as contact separation and tangential motion in two orthogonal directions for a CR implanted femur (first column) and a PS implanted femur (second column) at 48° flexion under normal fit conditions.

Fig. 4: Graphs highlighting the global peak motions for all implant and fit conditions investigated, a) and b) represent maximum and minimum peak motions in the first tangential direction (Cslip 1), whereas c) and d) represent maximum and minimum peak motions in the second tangential direction (Cslip 2). It is important to note that in the context of motion at the interface, maximum and minimum merely represent peak motions in opposite directions on the same surface.

Fig. 5: Femoral component relative motion expressed as contact separation and tangential motion in two orthogonal directions for a TS implanted femur with short stem (first column) and a TS implanted femur with long stem (second column) at 48° flexion under normal fit conditions.

Fig. 6: Femoral component relative motion expressed as contact separation and tangential motion in two orthogonal directions for a CR implanted femur (first column) and a PS implanted femur (second column) at 48° flexion under loose fit conditions.

Fig. 7: Femoral component relative motion expressed as contact separation and tangential motion in two orthogonal directions for a TS implanted femur with short stem (first column) and a TS implanted femur with long stem (second column) at 48° flexion under loose fit conditions.

Table 1: Material properties applied to finite element model. Cancellous and cortical bone properties were based on the manufacturer's specifications for the fourth generation composite femur, obtained from the Sawbones website: http://www.sawbones.com/UserFiles/Docs/biomechanical_catalog.pdf

Component	**Young's modulus E (N/mm^2)**	**Poisson's ratio (ν)**
Cortical bone	16700	0.3
Cancellous bone	155	0.3
Femoral component (Co-Cr)	210000	0.3
Femoral stem (ti-6al-4v)	110000	0.3

Table 2: Forces used in the FE analyses for the three flexion angles. Values were obtained from previous in-vivo telemetric implant studies [58, 59], normalised in terms of body weight and then applied to the FE model for an assumed average body weight of 775N.

	0°	**22°**	**48°**
Medial Force Fm (N)	436	1159	1160
Lateral Force FL (N)	291	772	773
Medial Anterior-Posterior force APm (N)	-57	130	-3
Lateral Anterior-Posterior force APl (N)	-57	130	-3
Patella-Femoral Force PF (N)	45	327	567
Internal-External moment IE (Nmm)	-829	3292	-7029

Table 3: Summary of the surface area calculated for each implant type at 0º flexion angle for four different bands of interface motion (0 – 20μm, 20 – 40μm, 40 – 80μm and 80 – 150μm). The value in brackets represents the percentage of the total surface area.

0º flexion		0 – 20μm (mm^2)	20 – 40μm (mm^2)	40 – 80μm (mm^2)	80 – 150μm (mm^2)
CR	Cslip 1	6728.54 (100)	0	0	0
	Cslip 2	6728.54 (100)	0	0	0
PS	Cslip 1	7467.70 (100)	0	0	0
	Cslip 2	7467.70 (100)	0	0	0
TSSS	Cslip 1	9908.77 (100)	0	0	0
	Cslip 2	9908.77 (100)	0	0	0
TSLS	Cslip 1	21870.12 (100)	0	0	0
	Cslip 2	21870.12 (100)	0	0	0
CR loose fit	Cslip 1	6924.06 (100)	0	0	0
	Cslip 2	6924.06 (100)	0	0	0
PS loose fit	Cslip 1	7632.53 (100)	0	0	0
	Cslip 2	7632.53 (100)	0	0	0
TSSS loose fit	Cslip 1	10073.04 (100)	0	0	0
	Cslip 2	10073.04 (100)	0	0	0
TSLS loose fit	Cslip 1	22038.98 (100)	0	0	0
	Cslip 2	22038.98 (100)	0	0	0

Table 4: Summary of the surface area calculated for each implant type at 22º flexion angle for four different bands of interface motion (0 – 20µm, 20 – 40µm, 40 – 80µm and 80 – 150µm). The value in brackets represents the percentage of the total surface area.

22º flexion		0 – 20µm (mm^2)	20 – 40µm (mm^2)	40 – 80µm (mm^2)	80 – 150µm (mm^2)
CR	Cslip 1	6721.85 (99.90)	6.69 (0.10)	0	0
	Cslip 2	6564.37 (97.56)	164.16 (2.44)	0	0
PS	Cslip 1	7421.47 (99.38)	46.23 (0.62)	0	0
	Cslip 2	7443.68 (99.68)	24.02 (0.32)	0	0
TSSS	Cslip 1	9857.43 (99.48)	51.34 (0.52)	0	0
	Cslip 2	9760.70 (98.51)	120.76 (1.22)	27.31 (0.28)	0
TSLS	Cslip 1	21867.95 (99.99)	2.17 (0.01)	0	0
	Cslip 2	21861.33 (99.96)	8.79 (0.04)	0	0
CR loose fit	Cslip 1	6917.32 (99.90)	6.74 (0.1)	0	0
	Cslip 2	6789.63 (98.06)	134.43 (1.94)	0	0
PS loose fit	Cslip 1	7507.67 (98.36)	124.86 (1.64)	0	0
	Cslip 2	7612.08 (99.73)	20.45 (0.24)	0	0
TSSS loose fit	Cslip 1	9943.26 (98.71)	129.78 (1.29)	0	0
	Cslip 2	10049.35 (99.76)	23.69 (0.24)	0	0
TSLS loose fit	Cslip 1	22031.60 (99.97)	7.37 (0.03)	0	0
	Cslip 2	22008.10 (99.86)	30.88 (0.14)	0	0

Table 5: Summary of the surface area calculated for each implant type at 48º flexion angle for four different bands of interface motion (0 – 20μm, 20 – 40μm, 40 – 80μm and 80 – 150μm). The value in brackets represents the percentage of the total surface area.

48º flexion		0 – 20μm (mm^2)	20 – 40μm (mm^2)	40 – 80μm (mm^2)	80 – 150μm (mm^2)
CR	Cslip 1	6395.00 (95.04)	254.44 (3.78)	79.10 (1.18)	0
	Cslip 2	6381.43 (94.84)	338.82 (5.04)	8.28 (0.12)	0
PS	Cslip 1	7001.12 (93.75)	297.80 (3.99)	168.78 (2.26)	0
	Cslip 2	7412.94 (99.27)	54.76 (0.73)	0.00	0
TSSS	Cslip 1	9448.09 (95.35)	316.62 (3.20)	144.06 (1.45)	0
	Cslip 2	9672.21 (97.61)	164.84 (1.66)	70.27 (0.71)	1.45 (0.01)
TSLS	Cslip 1	21603.84 (98.78)	266.28 (1.22)	0.00	0
	Cslip 2	21823.22 (99.79)	46.91 (0.21)	0.00	0
CR loose fit	Cslip 1	6589.96 (95.17)	223.31 (3.23)	110.79 (1.60)	0
	Cslip 2	6582.37 (95.07)	341.69 (4.93)	0.00	0
PS loose fit	Cslip 1	7046.10 (92.32)	361.38 (4.73)	221.74 (2.91)	3.31 (0.04)
	Cslip 2	7074.69 (92.69)	557.84 (7.31)	0.00	0
TSSS loose fit	Cslip 1	9569.00 (95.00)	325.60 (3.23)	173.18 (1.72)	5.26 (0.05)
	Cslip 2	9990.01 (99.18)	71.30 (0.71)	11.73 (0.12)	0
TSLS loose fit	Cslip 1	21663.88 (98.30)	280.40 (1.27)	94.70 (0.43)	0
	Cslip 2	21970.29 (99.69)	66.48 (0.30)	2.20 (0.01)	0

a)

b)

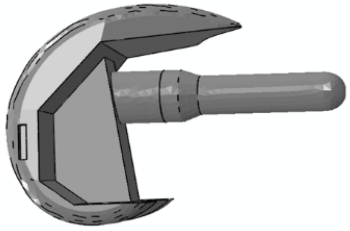

c)

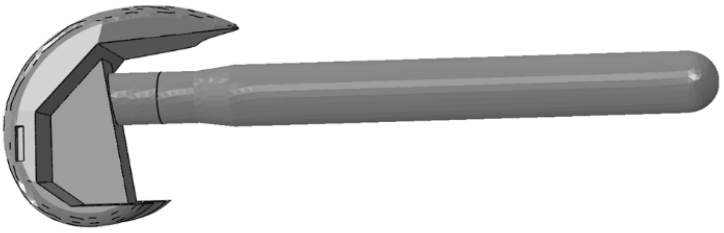

d)

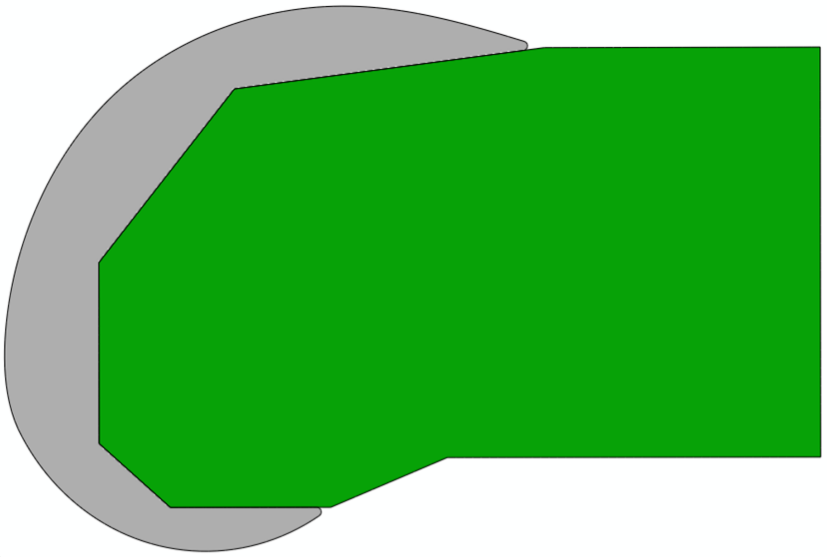

a)

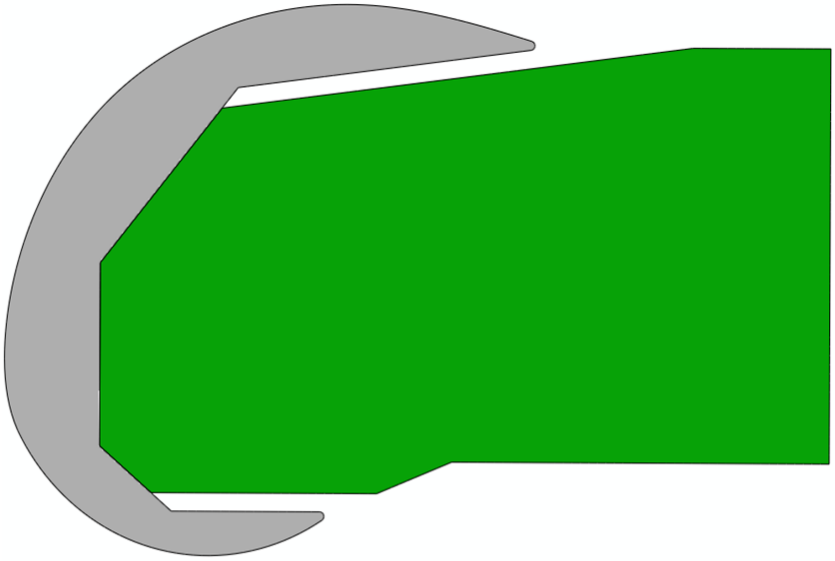

b)

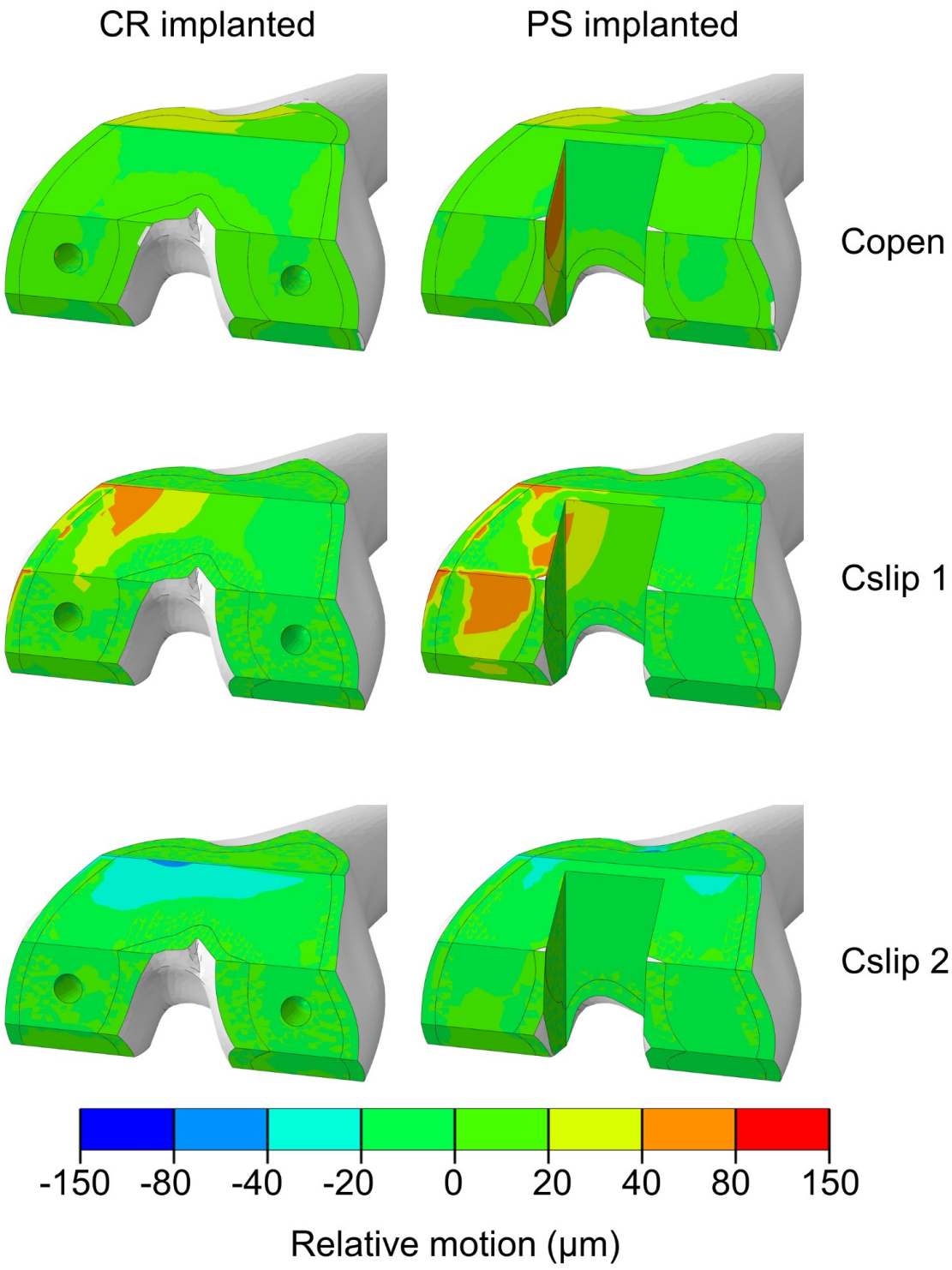
CR implanted
PS implanted
Copen
Cslip 1
Cslip 2
-150
-80
-40
-20
0
20
40
80
150
Relative motion (μm)

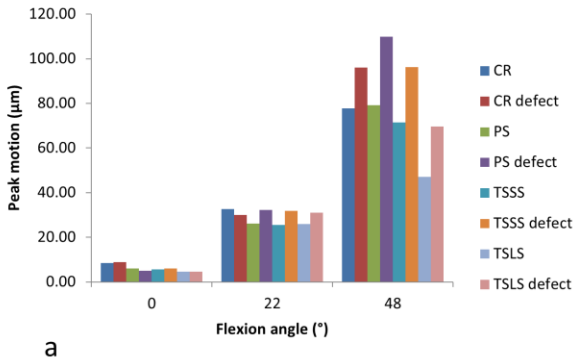
120.00
100.00
80.00
60.00
40.00
20.00
0.00
Peak motion (µm)
0
22
48
Flexion angle (°)
CR
CR defect
PS
PS defect
TSSS
TSSS defect
TSLS
TSLS defect

a

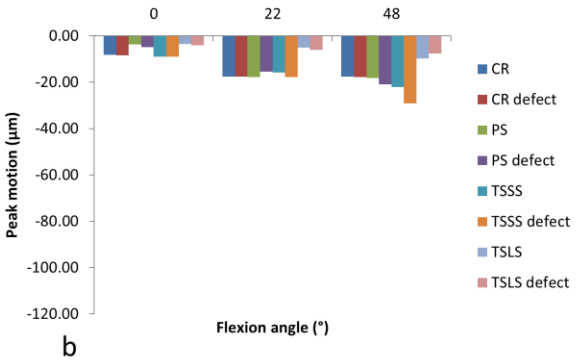
0
22
48
0.00
-20.00
-40.00
-60.00
-80.00
-100.00
-120.00
Peak motion (µm)
Flexion angle (°)
CR
CR defect
PS
PS defect
TSSS
TSSS defect
TSLS
TSLS defect

b

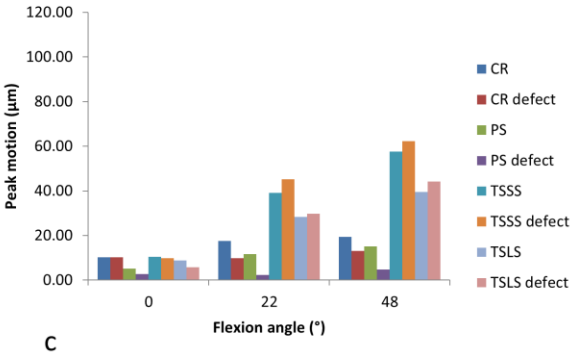
120.00
100.00
80.00
60.00
40.00
20.00
0.00
Peak motion (µm)
0
22
48
Flexion angle (°)
CR
CR defect
PS
PS defect
TSSS
TSSS defect
TSLS
TSLS defect

c

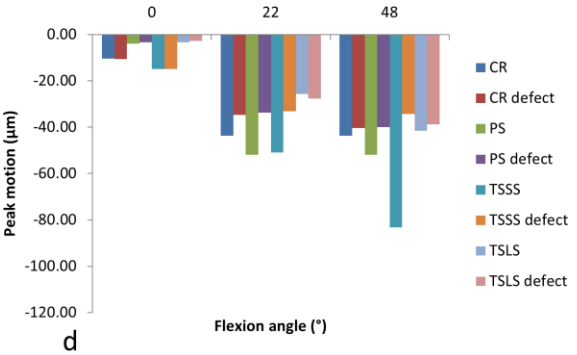
0
22
48
0.00
-20.00
-40.00
-60.00
-80.00
-100.00
-120.00
Peak motion (µm)
Flexion angle (°)
CR
CR defect
PS
PS defect
TSSS
TSSS defect
TSLS
TSLS defect

d

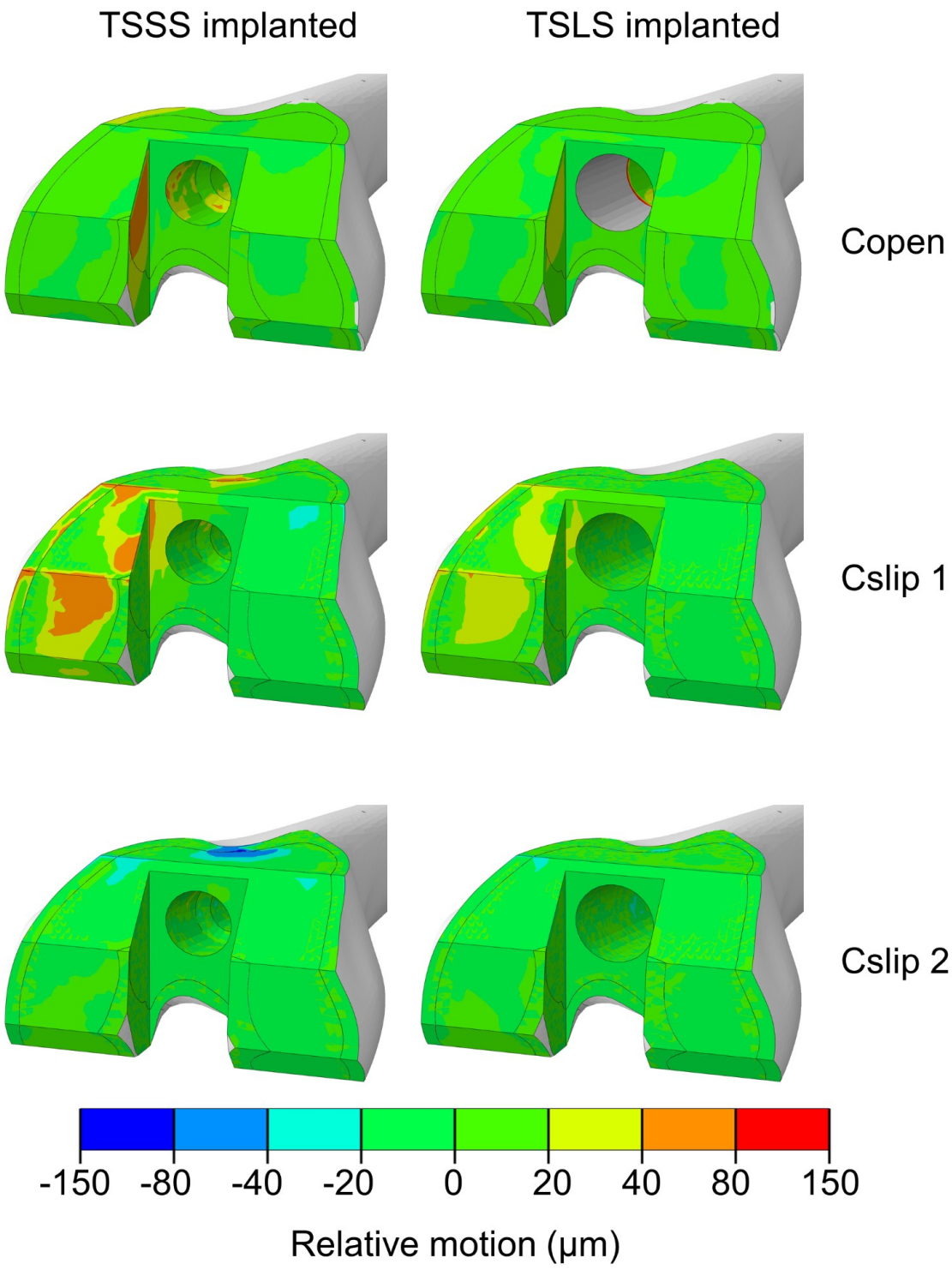
TSSS implanted
TSLS implanted
Copen
Cslip 1
Cslip 2
-150
-80
-40
-20
0
20
40
80
150
Relative motion (μm)

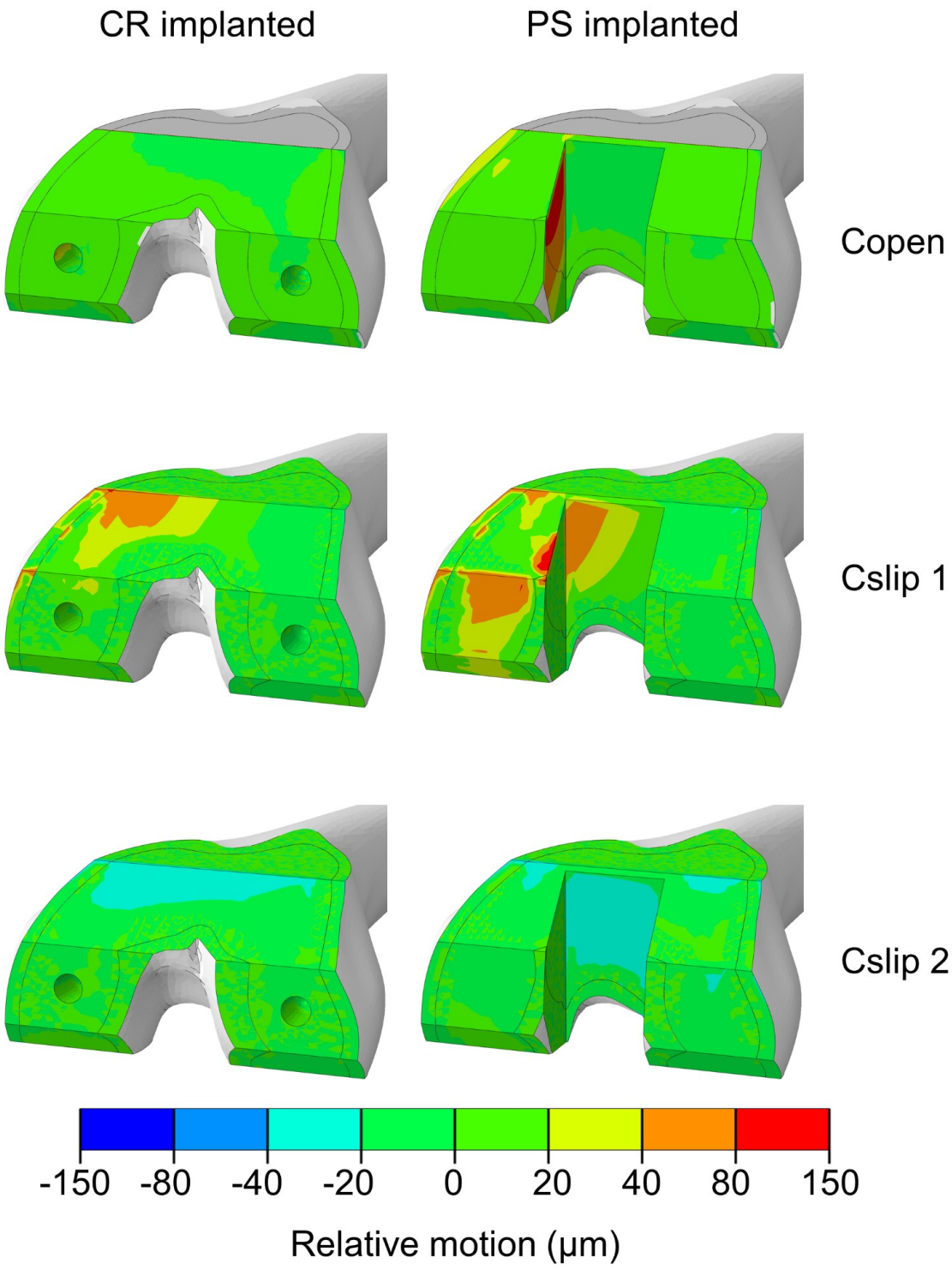
CR implanted
PS implanted
Copen
Cslip 1
Cslip 2
-150
-80
-40
-20
0
20
40
80
150
Relative motion (μm)

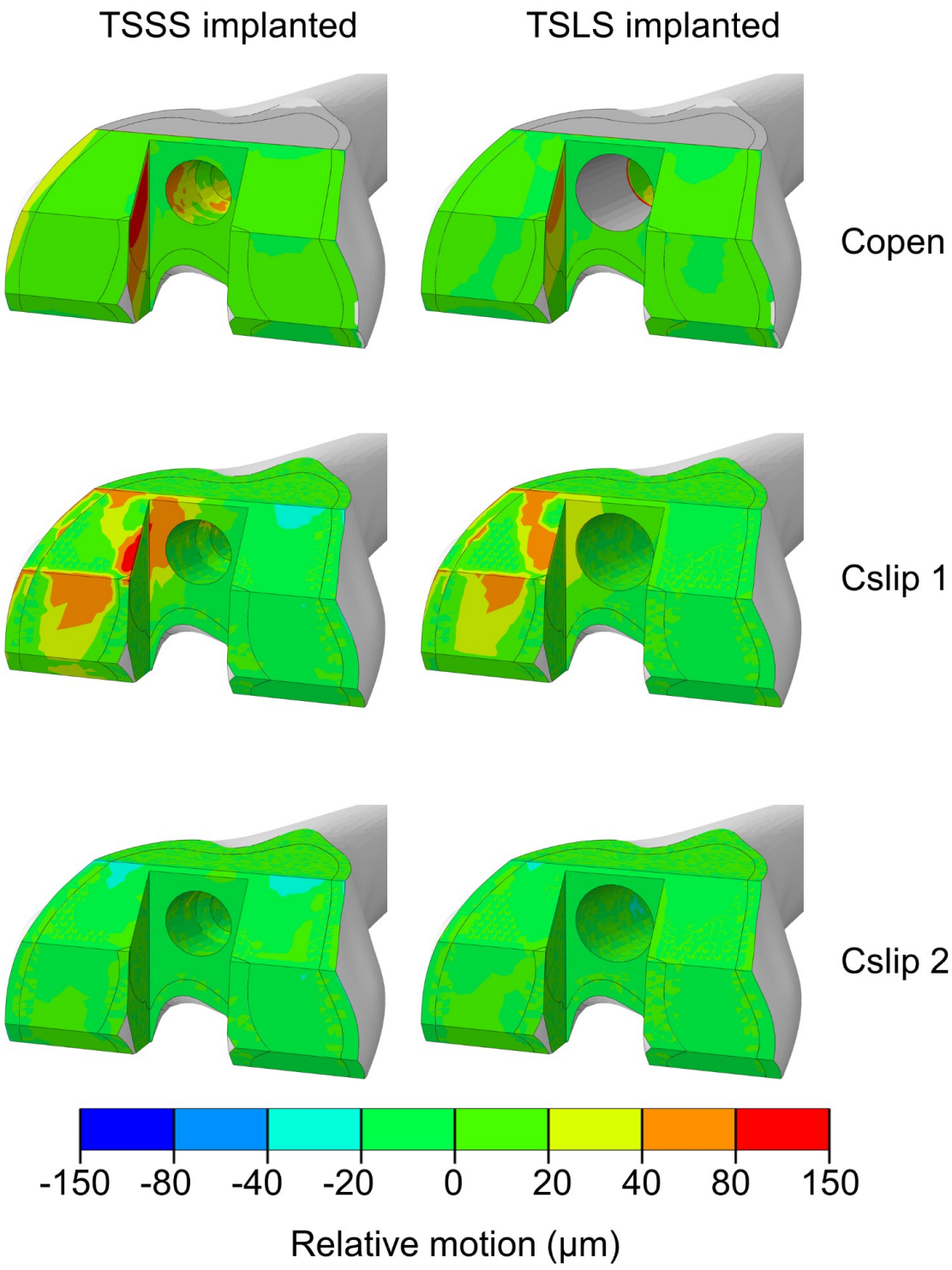
TSSS implanted
TSLS implanted
Copen
Cslip 1
Cslip 2
-150
-80
-40
-20
0
20
40
80
150
Relative motion (μm)